ACS APPLIED ENERGY MATERIALS
Article
Cite This: ACS Appl. Energy Mater. XXXX, XXX, XXX−XXX
www.acsaem.org

Plasma-Induced Fabrication and Straining of MoS_2 Films for the Hydrogen Evolution Reaction

Tianqi Liu,[†] Xinyu Liu,[†] Souvik Bhattacharya,[†] Zhipeng Ye,[§] Rui He,[§] Xuan P. A. Gao,[‡] Rohan Akolkar,[*,†] and R. Mohan Sankaran[*,†]

[†]Department of Chemical and Biomolecular Engineering and [‡]Department of Physics, Case Western Reserve University, Cleveland, Ohio 44106, United States

[§]Department of Electrical and Computer Engineering, Texas Tech University, Lubbock, Texas 79409, United States

Supporting Information

ABSTRACT: We present a novel plasma conversion process to fabricate strained MoS_2 films for the hydrogen evolution reaction (HER). Materials characterization of the initially converted film shows a rippled surface morphology that consequently contains in-plane and out-of-plane tensile strain. Smoothening of the films and relaxation of the strain are demonstrated by postsynthesis thermal treatment. Only negligible sulfur vacancies are detected in both the initially converted and thermally treated films. Electrochemical characterization shows that our plasma-converted, strained MoS_2 films are as intrinsically HER active as those produced by generating sulfur vacancies via postsynthesis plasma treatment. The reduced number of processing steps and direct, transfer-free growth enable a simple and scalable approach for fabricating MoS_2-based catalysts.

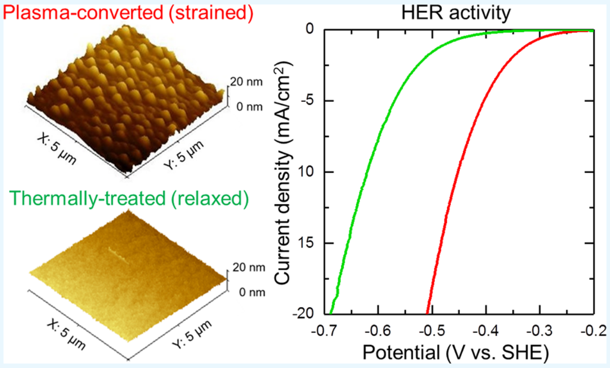

KEYWORDS: *molybdenum disulfide (MoS_2), plasma, hydrogen evolution reaction (HER), strain*

INTRODUCTION

Layered transition metal dichalcogenides (TMDs) such as molybdenum disulfide (MoS_2) are an earth-abundant and low-cost alternative to platinum catalysts for the hydrogen evolution reaction (HER) in electrochemical water splitting.[1,2] In the more common 2H phase of MoS_2, the origin of activity is diverse but can be classified by the type of structural defect.[3] The most prominent and well-studied are one-dimensional defects at the edges which have been theoretically[4] and experimentally[5] shown to be HER active and have been amplified by surface structuring to improve catalytic performance.[6] More recently, the possibility of creating zero-dimensional defects in the inert basal plane by generating sulfur vacancies where the undercoordinated Mo atoms introduce gap states that enhance hydrogen binding has been demonstrated.[7] Finally, it is also possible to have two-dimensional defects by mechanical deformation, which introduces tensile strain.[7−9] To fully realize MoS_2 catalysts in large-scale HER applications, facile, controllable, and scalable routes to generating these different types of defects are still needed.

One of the possibilities for generating defects in MoS_2 is plasma engineering. Plasmas contain charged species such as ions and electrons that can be accelerated by electric fields to high energies (>10 eV) to bombard a film surface and create cracks or holes to expose edges[10] or kick off sulfur atoms and produce vacancies.[7] With the addition of reactive gases such as oxygen, plasma treatment can also lead to the formation of new chemical bonds.[11] The plasma exposure is usually carried out postsynthesis on MoS_2 crystals initially obtained by exfoliation or chemical vapor deposition (CVD). The approach does not allow independent control over the different types of defects and is often only effective for flat surfaces because of the directionality of the charged species.[12] In addition, among the different structural changes that have been induced by a plasma, strain has not yet been demonstrated.

Here, we present a plasma process for synthesizing MoS_2 films while simultaneously generating defects in the form of tensile strain. Various postsynthesis thermal and plasma treatments were also applied to alter the film morphology and ultimately reveal the origin of HER activity in the as-grown films. Materials analysis showed that the as-grown MoS_2 films have a rough, nanostructured, rippled surface morphology and exhibit in-plane and out-of-plane strain but do not contain sulfur vacancies typical of postsynthesis plasma treatment. Thermal treatment was found to relax the strain and, at high temperatures of 1000 °C, produce smooth and highly crystalline films. In comparison, postsynthesis plasma treat-

Received: April 29, 2019
Accepted: June 18, 2019
Published: June 18, 2019

ment increased the film roughness and generated sulfur vacancies. Electrochemical characterization was performed, and the intrinsic HER activities of all the films were obtained by carrying out capacitance measurements to determine the electrochemically active surface areas. We find that thermal treatment reduces the intrinsic activity, consistent with the presence of strain in the as-grown films, and postsynthesis plasma treatment has a higher intrinsic activity than thermal treatment because of sulfur vacancies but is comparable to the as-grown films. Overall, our study demonstrates a simple and scalable approach to engineering strain in MoS_2 films to enhance HER activity.

EXPERIMENTAL SECTION

Synthesis of MoS_2 Films. MoS_2 thin films were synthesized by a process which we term plasma-enhanced chemical film conversion (PECFC), similar to that previously reported for h-BN.[13] Ammonium tetrathiomolybdate (ATM, Sigma-Aldrich) was first dissolved in 10 mL of dimethylformamide (DMF, Fisher Scientific) at 0.1 M with 0.1 g of 10000 MW linear polyethylenimine (L-PEI, Sigma-Aldrich) and sonicated at 60 °C for 1 h to completely dissolve the polymer. For materials analysis, the precursor solution was spin-coated on p-doped silicon (Si) substrates with 300 nm thick silicon dioxide (SiO_2) at 3000 rpm for 30 s. For HER testing, the precursor solution was spin-coated on both sides of a 1 cm × 1 cm Cu foil, cleaned by etching in 1 M H_2SO_4 to strip the oxide layer, at 3000 rpm for 30 s. After spin coating, the precursor films were dried in a vacuum oven for 30 min. To convert the precursor to MoS_2, the film was treated by a plasma generated in a homemade atmospheric-pressure reactor as a DBD in a parallel plate geometry by using high-voltage AC for 1 h. The background gas was a mixture of Ar and H_2 at a ratio of 80:20 flowing through the reactor at 100 sccm. The substrate was heated during plasma exposure by a 1 in. diameter microheater (MHI, Inc.). In addition to this initial plasma conversion step, films were also treated postsynthesis thermally in background Ar by using the same substrate heater for 30 min, thermally followed by exposure to the DBD in background Ar for 1 h, and thermally followed by exposure to a commercial low pressure parallel plate RF plasma (March Instruments PX250 System) at 100 W for 5 min.

AFM Characterization. Atomic force microscopy (AFM) images of the synthesized MoS_2 films were obtained by using an Agilent 5500 scanning probe microscope. The MoS_2 films were grown on a Si substrate to ensure a smooth background for imaging.

XPS Characterization. X-ray photoelectron spectroscopy (XPS) of the synthesized MoS_2 films was performed by using a PHI Versaprobe 5000 with an Al $K\alpha$ source. The stoichiometric ratios of Mo to S in the films were estimated from the areas of the peaks corresponding to the Mo 3d and S 2p states. The peak positions were calibrated based on the C 1s peak at 284.8 eV corresponding to C−C bonding which was always present from adventitious carbon.

Raman Measurements. Raman measurements were conducted at room temperature using a Horiba LabRAM HR Evolution Raman microscope system. The laser excitation wavelength was 532 nm, and the power was kept below 0.8 mW to avoid damage to the MoS_2 films. A 100× objective lens focused the laser beam to a spot with a diameter of ~1 μm, and the scattered signal was dispersed by a 1800 grooves/mm grating which provided an instrument resolution of ~0.5 cm^{-1}.

TEM Characterization. Transmission electron microscopy (TEM) images of the synthesized MoS_2 films were obtained by using a FEI Tecnai F30 operated at 300 kV. TEM samples were prepared by transferring the thin films from a Si substrate. The Si substrate was first removed by etching in a 30 wt % KOH solution for 3 h, followed by scooping the floating, free-standing film onto a carbon-coated Cu TEM grid.

Electrochemical Measurements. A conventional three-electrode setup was employed to measure HER activity from the synthesized MoS_2 films. The MoS_2 films were directly grown on both sides of 1 cm × 1 cm Cu foils for a total projected surface area of 2 cm^2 and served as the working electrode. A saturated calomel electrode (SCE) and a Pt wire were used as the reference and counter electrode, respectively. The electrolyte was 0.5 M H_2SO_4 (Fisher Scientific). Prior to measurements, the electrolyte was sparged with Ar for 30 min to remove dissolved oxygen. Linear sweep voltammetry was performed with an Ametek VersaSTAT 4 potentiostat at a slow scan rate of 2 mV/s. All electrochemical data were IR_{ohm}-corrected, and the electrolyte ohmic resistance, R_{ohm}, was estimated to be 2.9 Ω. To assess the surface area of the MoS_2 film, the double-layer capacitance was measured by cyclic voltammetry (CV) at different scan rates (20, 40, 80, and 160 mV/s). The anodic and cathodic potential limits during CV were 0.05 V and −0.15 V (vs SHE), respectively.

RESULTS AND DISCUSSION

Our strategy for synthesizing MoS_2 films was similar to previously reported for h-BN and is described in Figure 1a.

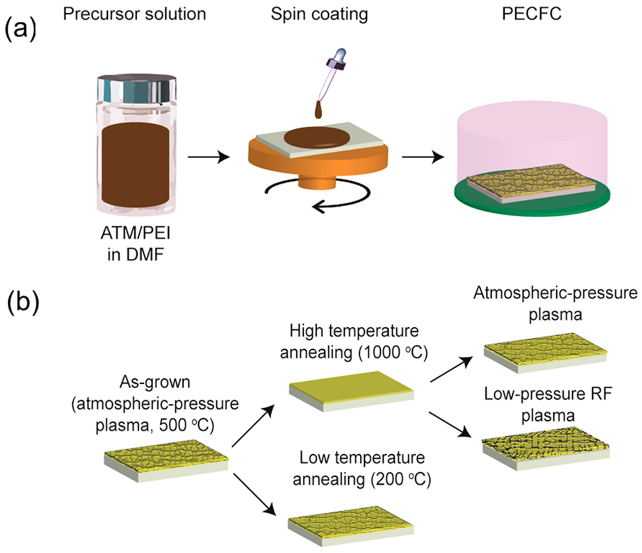

Figure 1. (a) Process flow diagram for PECFC synthesis of MoS_2 films consisting of the following steps: preparation of precursor solution containing a mixture of ammonium tetrathiolmolybdate (ATM) and linear polyethylenimine (L-PEI) in dimethylformamide (DMF), spin-coating of precursor solution onto a desired substrate followed by drying (not shown), and plasma treatment at atmospheric pressure with substrate heating typically at 500 °C. (b) Process flow diagram for various postsynthesis treatment steps of MoS_2 film grown by PECFC.

Briefly, a precursor solution was initially prepared composed of the molecular building block for MoS_2, ATM, and a complexing anionic polymer, L-PEI (Figure 1a, left). Previously, the polymer has been shown to aid in uniform coating of the ATM precursor and decomposes completely at 400 °C without carbon residue.[14] Subsequently, a precursor thin film was obtained by spin coating with the thickness controlled by the concentration of ATM in the solution (Figure 1a, middle). Finally, the precursor film was converted to a MoS_2 thin film by a plasma process which we term PECFC at 500 °C in a background of Ar and H_2 gas (Figure 1a, right).

To alter the morphology and other properties of the MoS_2 thin films grown by PECFC, we investigated several postsynthesis processing steps. In Figure 1b, the different steps are summarized, starting from the as-grown MoS_2 film. Additional

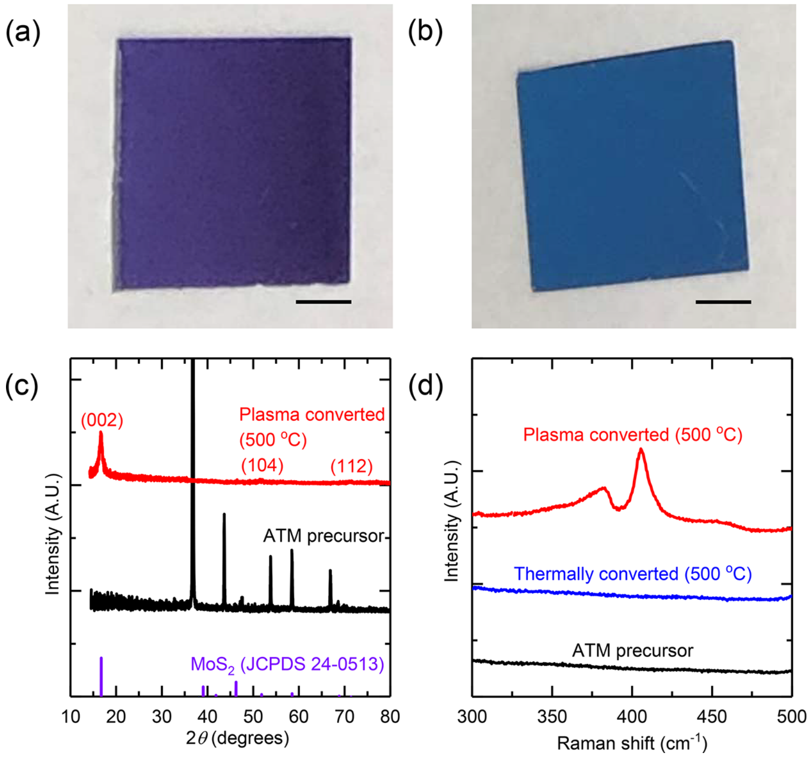

Figure 2. Optical images of ATM precursor film deposited and dried on SiO_2/Si (a) before conversion and (b) after conversion by plasma treatment at 500 °C. Scale bars are 3 mm. (c) X-ray diffraction (XRD) spectra of ATM precursor film before conversion (black) and after conversion by plasma treatment at 500 °C (red). The (002), (104), and (112) diffraction peaks are identified by matching with bulk hexagonal MoS_2 (JCPDS 24-0513, purple). (d) Representative micro-Raman spectra of ATM precursor film before (black) and after conversion by plasma (red) or thermal treatment (blue) at 500 °C. The E^1_{2g} and A_{1g} peaks corresponding to MoS_2 are only present in the plasma-treated film.

details of the processing steps are provided in the Supporting Information. The MoS_2 films were thermally treated in an inert gas at a high temperature of 1000 °C which was expected to anneal the strain and sinter smaller grains in the film, leading to larger grains and higher crystallinity. We also performed the thermal treatment at a lower temperature of 200 °C to relax the strain without allowing grain growth or change in the morphology.[15,16] The films were treated by a Ar plasma to generate sulfur vacancy defect sites by high-energy bombardment. We chose the MoS_2 films thermally treated at 1000 °C which should be the smoothest and highest crystalline quality to serve as a well-defined starting material for the plasma treatments. Two types of plasmas were utilized: a low-pressure RF plasma and the same atmospheric-pressure DBD employed for the initial synthesis step. The lower pressure and higher powers available in the RF plasma produce higher energies and fluxes of species at the film surface than the DBD which should lead to more sulfur vacancies.

We initially characterized the MoS_2 films grown by PECFC. Figures 2a and 2b show optical images of the ATM precursor film spin-coated onto 1 × 1 cm^2 Si substrates before and after conversion, respectively. Before conversion, the film is found to uniformly and continuously cover the substrate and appear purple. After conversion, the film remains uniform and continuous, showing that the plasma treatment did not cause significant sputtering or etching but appears blue, which is indicative of conversion to MoS_2. The homogeneity of the film after conversion was further confirmed under an optical microscope (Figure S1a). The thickness of this film was measured to be ∼30 nm by AFM (Figure S1b). In general, the film thickness depended on the concentration of the precursor in the spin-coating solution and was limited to >20 nm to avoid film discontinuities after spin coating, which based on an interlayer distance of 0.67 nm corresponds to ∼30 layers. Figure 2c shows XRD spectra of the ATM precursor film before and after conversion. The disappearance of peaks corresponding to the ATM precursor and the appearance of peaks indexed to bulk hexagonal MoS_2 (JCPDS 24-0513) following plasma treatment confirms complete conversion. We note that the penetration depth of XRD which is >10 μm was larger than the film thickness. After plasma conversion, the presence of small diffraction peaks corresponding to the (104) and (112) crystal planes in addition to the intense diffraction peak corresponding to the (002) crystal plane suggests that the multilayers are not perfectly aligned.[17] Layer alignment was improved by an additional thermal treatment step at 1000 °C as indicated by a narrower and higher intensity (002) diffraction peak and disappearance of the (104) and (112) diffraction peaks (Figure S2). Micro-Raman spectroscopy provided further evidence for conversion of the ATM precursor films to MoS_2, with spectra showing new peaks at ∼381.5 and ∼406.9 nm, respectively, after plasma treatment corresponding to the in-plane optical phonon mode with E^1_{2g} and A_{1g} symmetry of crystalline MoS_2 (Figure 2d).[18] The difference in these peak positions has been shown to increase monotonically with the number of layers[19] and was found to correspond to a relatively thick film >6 layers, which is in good agreement with AFM analysis. Interestingly, we did not observe conversion without the presence of the plasma (heating only) (see Figure 2d) as has been previously reported.[14,15] There are several differences that could explain the lack of conversion. Liu et al. found that sapphire instead of

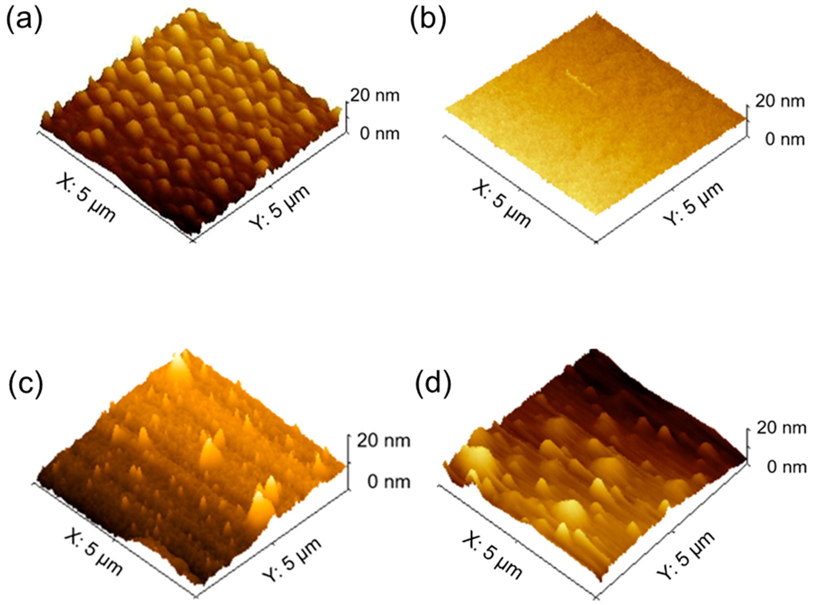

Figure 3. AFM images of (a) as-grown MoS_2 film synthesized by PECFC at 500 °C, (b) MoS_2 film after high-temperature thermal treatment at 1000 °C of as-grown MoS_2 film, (c) after atmospheric-pressure plasma treatment of high-temperature, thermally treated MoS_2 film, and (d) low-pressure RF plasma treatment of high-temperature, thermally treated MoS_2 film.

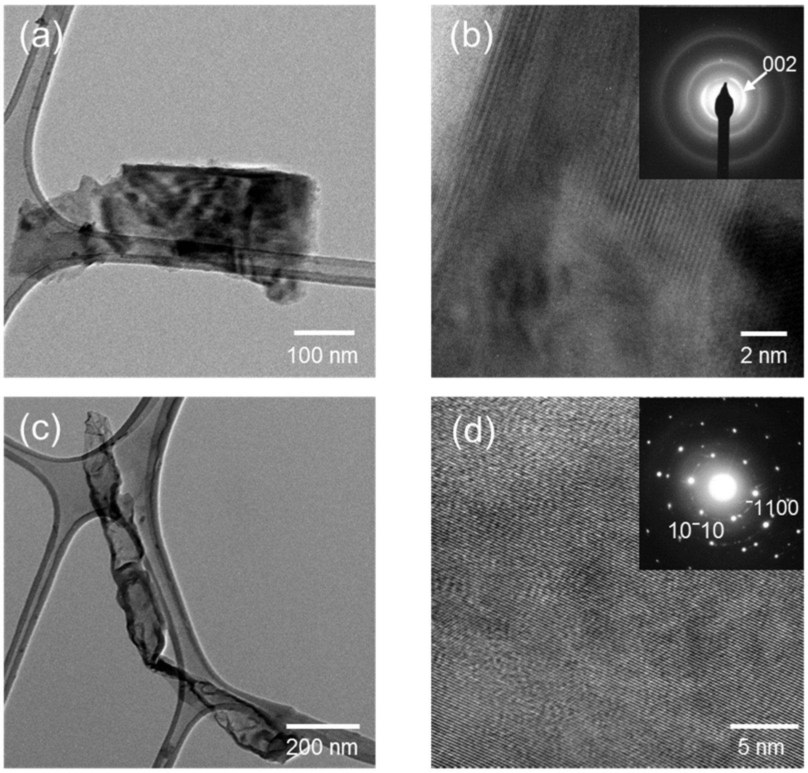

Figure 4. (a) Low-magnification and (b) high-magnification images of as-grown MoS_2 film synthesized by PECFC at 500 °C. The SAED pattern of the corresponding film is shown in the inset of (b). (c) Low-magnification and (d) high-magnification images after high-temperature thermal treatment of as-grown MoS_2 film. The SAED pattern of the corresponding film is shown in the inset of (d) with the (10−10) and (−1100) lattice planes identified.

SiO_2/Si and two thermal treatment steps, the first at lower temperature similar to ours (500 °C) and the second at higher temperature (1000 °C) and with the addition of sulfur vapor, improved conversion.[15] Yang et al. incorporated a polymer, L-PEI, to reduce dewetting of the ATM precursor and avoid sulfurization and performed the conversion in a single thermal treatment step with a rapid thermal annealing system at a slightly higher temperature than ours (700 °C).[14] In both studies, the thermolysis was performed at vacuum pressures (~1 Torr). On the basis of these differences, we suggest that the polymer, L-PEI, impedes reactions that allow MoS_2 nucleation and growth, necessitating higher temperatures

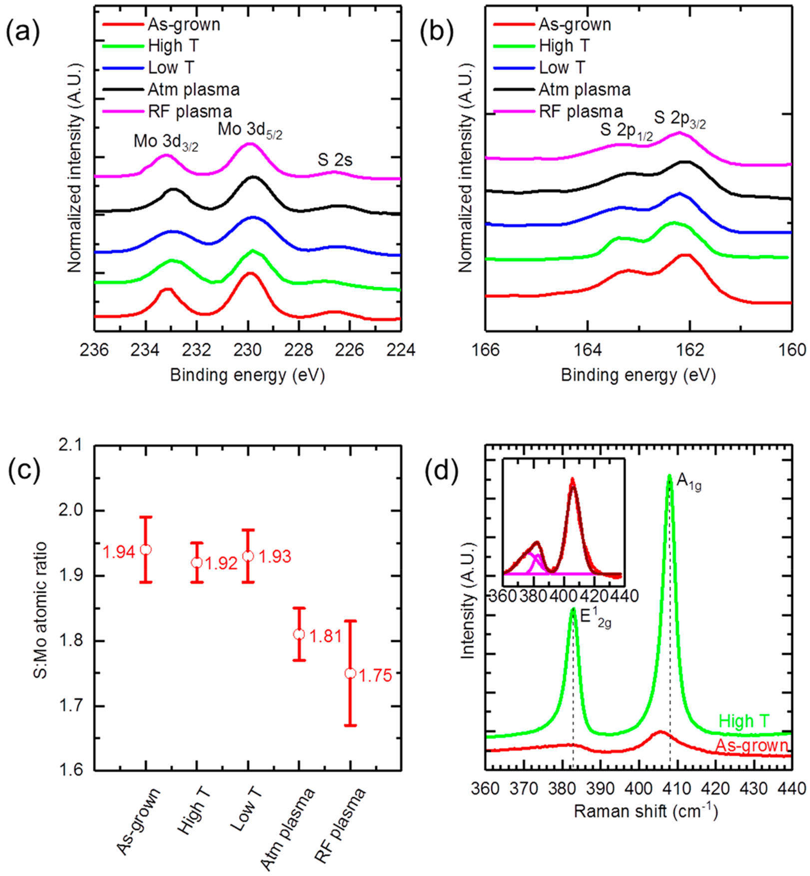

Figure 5. XPS spectra of the (a) Mo 3d and (b) S 2p binding energy range of as-grown and postsynthesis treated MoS_2 films (details of the films are shown in Figure 1b). (c) Average atomic ratio of S:Mo in as-grown and postsynthesis treated MoS_2 films. The error bars correspond to the variance within one standard deviation in the measurements from ∼3 spots across each film. (d) Representative micro-Raman spectra of as-grown and high-temperature thermally treated MoS_2 films. The inset shows a close-up of the spectrum for the as-grown sample with the A_{1g} and E^1_{2g} peaks fitted by Gaussian line shapes. The red line is the original spectrum, the brown line is the fitted overall spectrum, and the pink lines are the deconvolution of the E^1_{2g} peak into two sub-bands.

and/or lower pressures. Our results show that the addition of a plasma enables conversion at lower temperatures and higher (atmospheric) pressure.

The surface morphology of the MoS_2 films grown by PECFC and following the various postsynthesis treatments was characterized by AFM. Figure 3a shows that the initially converted MoS_2 thin film exhibits a relatively rough and nanostructured surface, reflected by a RMS roughness of 1.7 nm. The morphology could be the result of bombardment by plasma species during growth or the mechanism underlying the MoS_2 crystal growth whereby a mismatched lattice constant with that of the substrate or thermal expansion/compression from temperature gradients led to rippled nanostructures.[20] After thermally treating at 1000 °C, the surface becomes extremely smooth with a RMS roughness of 0.5 nm (Figure 3b), which is comparable to some of the smoothest films reported.[21,22] In comparison, thermally treating at 200 °C had minimal effect on the nanostructure morphology, increasing the RMS roughness from 1.7 to 1.9 nm (Figure S3a). Thermal treatment at temperatures higher than 200 °C was found to alter the surface morphology (Figure S3b,c). The postsynthesis plasma treatments were found to more substantially increase the surface roughness, with the RMS increasing in our high temperature treated films from 0.5 to 3.5 nm for the RF plasma (Figure 3c) and to 1.6 nm for the DBD (Figure 3d). The larger increase for the RF plasma supports the presence of higher energy species. Previous reports of postsynthesis plasma treatment by a similar plasma have shown that the bombardment of the species on the film leads to removal of material and, in some cases, even the formation of cracks and holes.[10] There could also be redeposition of material at the surface. However, the surface temperature remains close to room temperature in these nonthermal plasmas, and even if the material redeposits, there should not be any diffusion of these moieties and the film surface will become increasingly rough, in agreement with AFM measurements.

The MoS_2 films grown by PECFC and after high temperature treatment, two of the more different morphologies, were further characterized at the atomic scale by TEM. Figure 4a shows a low-magnification image of an ∼ 150 nm × 300 nm section transferred from the initially converted thin film. The high-resolution image and corresponding selected area electron diffraction (SAED) in Figure 4b reveal that the film is nanocrystalline, composed of a network of relatively small crystal grains and amorphous regions. Figure 4c shows a low-magnification TEM image of an ∼100 nm × 1 μm section transferred from a film after high-temperature thermal treatment. In comparison, the film was found to exhibit a higher crystalline quality as evident from the high-resolution image in Figure 4d and the corresponding SAED which displays a single hexagonal orientation characterized by the (−1100) and (10−10) lattice planes. The grain size was

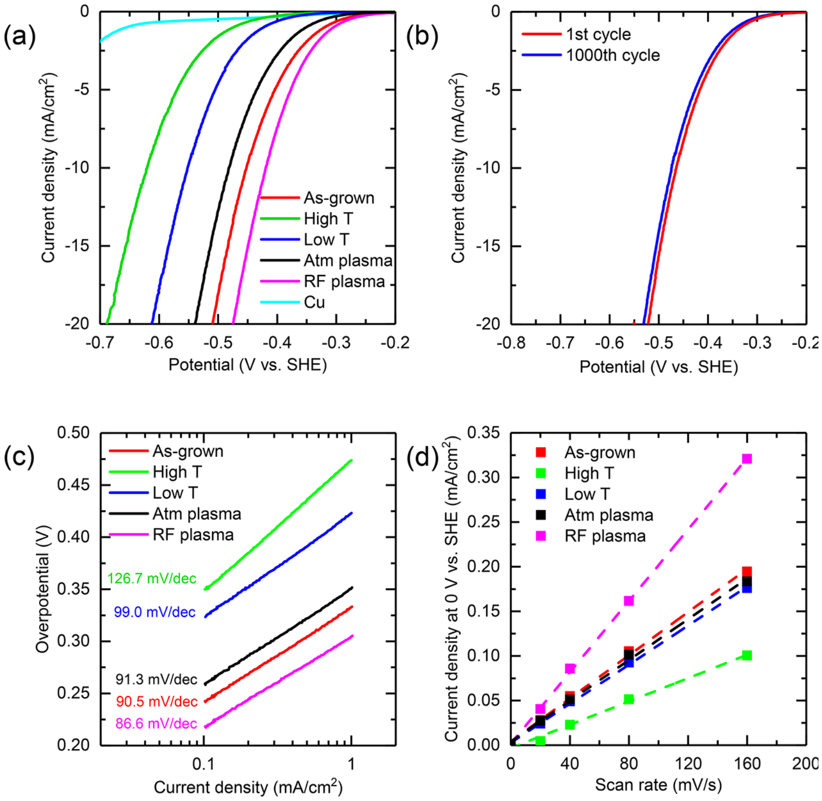

Figure 6. (a) Polarization curves of as-grown and postsynthesis treated MoS_2 films (details of the films are shown in Figure 1b). (b) Durability test of as-grown MoS_2 film (20 s/cycle). (c) Tafel plots of as-grown and postsynthesis treated MoS_2 films. (d) Electrochemical double-layer capacitance measurements of as-grown and postsynthesis treated MoS_2 films.

measured to be >30 nm, which compares favorably with some of the highest quality films produced by CVD.[23,24] A cross-sectional TEM image reveals the layered structure over a thickness of ~25 nm (Figure S4). The improved morphology and crystallinity of the converted MoS_2 films after high temperature thermal treatment agree well with AFM analysis.

The chemical composition of the MoS_2 films grown by PECFC and after different postsynthesis treatments was assessed by XPS. Figures 5a and 5b show the Mo 3d and S 2p binding energy regions for a series of samples normalized by the integrated area of the Mo 3d peaks. The locations of the Mo peaks at ~229.8 and ~233.0 eV correspond to the Mo $3d_{5/2}$ and Mo $3d_{3/2}$ binding energies, respectively, and the locations of the S peaks at ~162.2 and ~163.4 eV correspond to the S $2p_{3/2}$ and S $2p_{1/2}$ binding energies, respectively. These binding energies match well with MoS_2, confirming that all the films are essentially MoS_2. The Mo 3d peak intensities were observed to be almost unchanged from the initially grown film for all the postsynthesis treatments, indicating that the ATM precursor is fully converted to Mo^{4+} without any MoS_3 intermediate, even after the initial plasma treatment step. This is in agreement with other reported work that in the presence of H_2, ammonium tetrathiomolybdate will be converted into MoS_2 at 500 °C.[25] On the other hand, the S 2p peak intensities appear to change after some of the postsynthesis treatment steps. To more carefully quantify this effect, the stoichiometric ratio of Mo to S was determined in the different samples from the peak areas by integrating the Mo 3d and S 2p peaks from 228.1 to 234.7 eV and 160.9 to 164.4 eV, respectively. Multiple XPS spectra were collected from ~3 spots across each film to calculate an average (Figures S5−S9). Figure 5c shows that the S:Mo atomic ratio of the initially converted film is 1.94:1, which is close to the ideal 2:1 ratio and indicates that there are a negligibly small amount of sulfur vacancies. Thermal treatment at high and low temperatures does not appreciably change the ratio, with high temperatures giving a value of 1.92 and low temperatures giving a value of 1.93. However, plasma treatment significantly changes the ratio with a RF plasma decreasing the ratio to 1.75 and a DBD decreasing the ratio to 1.81. The lower ratio is directly related to the expected generation of sulfur vacancies, and the increased generation by the RF plasma is consistent with our picture of higher energy and flux of species to the film surface as well as previous reports.[7,10,11] Interestingly, the same DBD is only found to generate sulfur vacancies postsynthesis and not during the initial conversion step. We suggest that during conversion the sulfur-rich ATM precursor $[(NH_4)_2MoS_4]$ produces a vapor layer enriched in sulfur moieties including hydrogen sulfide (H_2S) which prevent vacancies from forming similar to how sulfur vapor has been added in prior experiments during film conversion.[15,26]

Another potential structural defect in the MoS_2 films is tensile strain which can be characterized by micro-Raman spectroscopy.[27,28] Figure 5d displays representative Raman spectra from the initially converted MoS_2 film (as-grown) and from MoS_2 after high-temperature treatment. The A_{1g} and E^1_{2g} Raman peaks are observed to be much sharper after high-temperature treatment, indicating the formation of high crystalline quality MoS_2. The inset of Figure 5d shows a zoomed-in image of the spectrum for as-grown MoS_2. The E^1_{2g} peak shows an asymmetric line shape and can be decomposed into two sub-bands, which suggests the presence of large in-plane tensile strain estimated to be >1% in the as-grown sample.[29] In addition, the A_{1g} Raman peak is blue-shifted by about 2 cm^{-1} after thermal treatment, suggesting that the as-grown MoS_2 also contains out-of-plane strain. The out-of-plane strain may be related to the multilayer structure which was found by XRD analysis to be more aligned following heating. The in-plane and out-of-plane strain, i.e., strain in all three dimensions, in the initially converted films can be correlated to the rippled morphology observed by AFM. Similar ripple structures were previously obtained by vapor deposition[20] and laser illumination,[30] and comparable strains of 0.1−0.6% were estimated.[20] Further evidence in support of a link between the ripples and strain is provided by the thermal treatment at higher temperatures of 1000 °C which was found by AFM analysis to eliminate the ripples and, concomitantly, by Raman analysis, the strain. We note that while as-grown MoS_2 films subjected to thermal treatment at lower temperatures of 200 °C and plasma treatments were found by AFM analysis to exhibit surface roughness, they were not characterized by the same rippled surface and, thus, would not be expected to be similarly strained.

The MoS_2 thin films were grown by PECFC directly without transfer on Cu substrates (Figure S10a,b) and subjected to the same postsynthesis treatments to be studied as catalysts for HER. The HER activity was evaluated by performing slow scan (2 mV/s) voltammetry in an aqueous 0.5 M H_2SO_4 electrolyte at room temperature to allow the system to be near steady state. Further evidence of near steady state was provided by the overlap between forward (going from anodic-to-cathodic potentials) and reverse (going from cathodic-to-anodic potentials) scans (Figure S11a). To ensure that dissolution of the Pt counter electrode and redeposition on the working electrode was not an issue,[31] we compared the polarization curve with a graphite counter electrode and found virtually no difference (Figure S11b). Figure 6a shows a comparison of the polarization curves where current density refers to the measured current normalized by the total projected area of the Cu substrate which was constant (2 cm^2). As expected, a bare Cu substrate showed low activity characterized by only a small HER current density (<2 mA/cm^2) over the entire potential range tested. All PECFC-fabricated MoS_2 films with various applied treatments showed higher activity. The strained, initially converted film was found to yield an overpotential of 465 mV at a current density of 10 mA/cm^2. Following thermal treatment which relaxed the strain, the overpotentials at the same current density increased to 620 mV for high temperature and to 552 mV for low temperature, reflecting a decrease in activity. Plasma treatment of the high-temperature-treated films was found to increase activity, with the RF plasma showing the lowest overall overpotential of 420 mV and the DBD showing an overpotential of 482 mV. The durability of the initially converted film was assessed by potential cycling. Figure 6b shows that there was only a slight decrease in activity (<5% decrease in current density at 400 mV) after 1000 cycles.

To provide further insight into the electrocatalytic activity of the MoS_2 thin films, Tafel plots were constructed (Figure 6c). In general, smaller Tafel slope values imply that the MoS_2 is more effective in catalyzing HER.[32] The ordering of the Tafel slopes was found to be exactly the same as the overpotentials discussed above; i.e., high-temperature treatment showed the largest slope (126.7 mV/dec), followed by low-temperature treatment (99.0 mV/dec), atmospheric-pressure plasma treatment of the high temperature treated film (91.3 mV/dec), and the initially converted film (90.5 mV/dec). The RF plasma treatment of the high-temperature-treated film exhibited the lowest Tafel slope (86.6 mV/dec).

There could be several contributions to the HER activity including the electrochemically active surface area and defective nature of the MoS_2 films. To understand the role of active surface area, electrochemical capacitance measurements were performed to determine the available electroactive area of the catalyst film.[23,33] Briefly, the double-layer charging current, i, is linearly related to both the scan rate, ν, and the electrochemically active surface area of the electrode. By obtaining CVs at different scan rates (Figure S12) and plotting the double-layer charging current at a given potential as a function of scan rate, as shown in Figure 6d, the active surface areas for the various MoS_2 films were compared. Our results show that the film after RF plasma treatment has the highest area and the film after high-temperature treatment has the smallest area, which is in excellent agreement with the morphology observed by AFM and TEM (see Figures 3 and 4).

Table 1. Summary of Electrochemical Parameters of MoS_2 Films for HER Application

sample	double-layer capacitance (mF/cm^2)	Tafel slope (mV/dec)	current at −0.5 V vs SHE (mA)	site density ($10^{15}/cm^2$)	TOF (H_2 s^{-1}/surface site)
as-grown	1.25	91	37.4	24.3	2.4
high *T*	0.63	127	3.2	12.1	0.4
low *T*	1.07	99	9.4	20.8	0.7
atm plasma	1.19	91	25.4	23.1	1.7
RF plasma	1.91	87	56.4	37.1	2.4

From the electrochemical measurements, the intrinsic HER activity normalized to the number of sites, i.e., the turnover frequency (TOF), can be estimated. Table 1 summarizes key electrochemical parameters measured and the TOF estimated for each of the MoS_2 films studied. Briefly, we first estimated the surface site density, N_{sites}, which refers to the number of sites available on MoS_2 for hydrogen adsorption, from the double-layer capacitance following the procedure outlined in previous reports.[33,34] Additional details of our calculations are provided in the Supporting Information. From the measured current, I (corresponding to 0.5 V in the polarization curve) and the surface site density, the TOF could be estimated via the following equation:

$$\mathrm{TOF} = \frac{IN_A}{nFA_{geo}N_{sites}} \tag{1}$$

where n refers to the number of electrons transferred and is 2 for HER, F is the Faraday constant, A_{geo} is the projected or geometric area of the Cu electrode and equals 2 cm^2, and N_A is the Avogadro constant. Our results show that the TOF is equally highest for the initially converted film and after RF plasma treatment (2.4) and is lowest after high-temperature treatment (0.41). Treatment at low temperature had minimal effect on the site density, in agreement with AFM analysis, but decreased the TOF substantially. In comparison, atmospheric and RF plasma treatments increased both the site density and the TOF. To allow a clearer comparison between the different films, we introduce a dimensionless ratio (ϕ):

$$\phi_{a-b} = \frac{[\mathrm{TOF}]_a}{[\mathrm{TOF}]_b} \tag{2}$$

where "a" and "b" refer to two samples being compared in Table 1. The importance of this parameter is that if $\phi_{a-b} > 1$, then site specific activity in sample "a" is higher than that in "b". For example, from Table 1, it can be observed that $\phi_{\text{High-}T\text{–As-grown}} = 0.17$ and $\phi_{\text{Low-}T\text{–As-grown}} = 0.29$, indicating that thermally treated films have sites with lower activity likely due to the removal of strain in the initially converted film. On the contrary, $\phi_{\text{RF-plasma–High-}T} = 6.0$, reflecting that site specific activity was significantly enhanced by RF plasma treatment consistent with the introduction of sulfur vacancies. While $\phi_{\text{RF-plasma–As-grown}} = 1.0$, we note that these two films are very different both in terms of how they are processed and their chemical and physical properties. Given that S vacancies are absent in the as-grown films (see Figure 5c) and the site specific activity decreases after thermal treatment, we can postulate that the high site specific activity for HER in these films originates from strain present in the film, consistent with our Raman analysis (see Figure 5d).

■ SUMMARY

In summary, we have developed a plasma conversion process to fabricate MoS_2 from solution-deposited precursor films and performed several postsynthesis treatments to alter the morphology and chemical composition. Materials analysis shows that the initially converted film is strained but contains negligible sulfur vacancies, and postsynthesis thermal treatment relaxes the strain and postsynthesis plasma treatment generates sulfur vacancies. These properties are linked to the HER activity of the films with the postsynthesis thermal treatment decreasing activity and postsynthesis plasma treatment increasing activity. The difference between the initial plasma conversion step and the postsynthesis plasma treatment is believed to be related to the presence of strain versus sulfur vacancies. In the future, both of these may need to be controlled to tune activity, not only for HER but also for other reactions and materials.

■ ASSOCIATED CONTENT

Ⓢ Supporting Information

The Supporting Information is available free of charge on the ACS Publications website at DOI: 10.1021/acsaem.9b00843.

> Experimental details for postsynthesis treatments, optical and AFM images of MoS_2 films grown by PECFC at 500 °C, XRD of MoS_2 film after plasma treatment at 500 °C followed by thermal treatment at 1000 °C, AFM image of MoS_2 grown by PECFC at 500 °C followed by thermal treatments at different temperatures, cross-sectional TEM image of MoS_2 film grown by PECFC at 500 °C, XPS spectra of MoS_2 films grown by PECFC at 500 °C, grown by PECFC at 500 °C followed by thermal treatment at 1000 °C, grown by PECFC at 500 °C followed by thermal treatment at 200 °C, grown by PECFC at 500 °C followed by thermal treatment at 1000 °C followed by atmospheric DBD treatment, grown by PECFC at 500 °C followed by thermal treatment at 1000 °C followed by low-pressure RF plasma treatment, optical images of ATM precursor film deposited on Cu substrate before and after PECFC at 500 °C, comparison of polarization curves for MoS_2 films with forward vs reverse potential scans and with Pt vs graphite counter electrodes, electrochemical capacitance measurements, and details of TOF calculation (PDF)

■ AUTHOR INFORMATION

Corresponding Authors

*E-mail mohan@case.edu.
*E-mail rna3@case.edu.

ORCID

Rui He: 0000-0002-2368-7269
Xuan P. A. Gao: 0000-0002-7045-9656
R. Mohan Sankaran: 0000-0002-9399-4790

Notes

The authors declare no competing financial interest.

■ ACKNOWLEDGMENTS

This work was financially supported by the National Science Foundation (NSF) under Grant DMR-1708742. Z.Y. and R.H. acknowledge support from NSF CAREER Grant DMR-1760668.

■ REFERENCES

(1) Voiry, D.; Salehi, M.; Silva, R.; Fujita, T.; Chen, M.; Asefa, T.; Shenoy, V. B.; Eda, G.; Chhowalla, M. Conducting MoS_2 Nanosheets as Catalysts for Hydrogen Evolution Reaction. *Nano Lett.* **2013**, *13*, 6222−6227.

(2) Li, Y.; Wang, H.; Xie, L.; Liang, Y.; Hong, G.; Dai, H. MoS_2 Nanoparticles Grown on Graphene: an Advanced Catalyst for the Hydrogen Evolution Reaction. *J. Am. Chem. Soc.* **2011**, *133*, 7296−7299.

(3) Lin, Z.; Carvalho, B. R; Kahn, E.; Lv, R.; Rao, R.; Terrones, H.; Pimenta, M. A; Terrones, M. Defect Engineering of Two-Dimensional Transition Metal Dichalcogenides. *2D Mater.* **2016**, *3*, 022002.

(4) Hinnemann, B.; Moses, P. G.; Bonde, J.; Jorgensen, K. P.; Nielsen, J. H.; Horch, S.; Chorkendorff, I.; Norskov, J. K. Biomimetic Hydrogen Evolution: MoS_2 Nanoparticles as Catalyst for Hydrogen Evolution. *J. Am. Chem. Soc.* **2005**, *127*, 5308−5309.

(5) Jaramillo, T. F.; Jorgensen, K. P.; Bonde, J.; Nielsen, J. H.; Horch, S.; Chorkendorff, I. Identification of Actives Edge Sites for Electrochemical H_2 Evolution from MoS_2 Nanocatalysts. *Science* **2007**, *317*, 100−102.

(6) Kibsgaard, J.; Chen, Z.; Reinecke, B. N.; Jaramillo, T. F. Engineering the Surface Structure of MoS_2 to Preferentially Expose the Active Edge Sites for Electrocatalysis. *Nat. Mater.* **2012**, *11*, 963−969.

(7) Li, H.; Tsai, C.; Koh, A. L.; Cai, L.; Contryman, A. W.; Fragapane, A. H.; Zhao, J.; Han, H. S.; Manoharan, H. C.; Abild-Pedersen, F.; Nørskov, J. K.; Zheng, X. Activating and Optimizing MoS_2 Basal Planes for Hydrogen Evolution through the Formation of Strained Sulfur Vacancies. *Nat. Mater.* **2016**, *15*, 48−53.

(8) Li, H.; Du, M.; Mleczko, M. J.; Koh, A. L.; Nishi, Y.; Pop, E.; Bard, A. J.; Zheng, X. Kinetic Study of Hydrogen Evolution Reaction over Strained MoS_2 with Sulfur Vacancies Using Scanning Electrochemical Microscopy. *J. Am. Chem. Soc.* **2016**, *138*, 5123−5129.

(9) Lee, J. H.; Jang, W. S.; Han, S. W.; Baik, H. K. Efficient Hydrogen Evolution by Mechanically Strained MoS_2 Nanosheets. *Langmuir* **2014**, *30*, 9866−9873.

(10) Ye, G.; Gong, Y.; Lin, J.; Li, B.; He, Y.; Pantelides, S. T.; Zhou, W.; Vajtai, R.; Ajayan, P. M. Defects Engineered Monolayer MoS_2 for Improved Hydrogen Evolution Reaction. *Nano Lett.* **2016**, *16*, 1097−1103.

(11) Tao, L.; Duan, X.; Wang, C.; Duan, X.; Wang, S. Plasma-Engineered MoS_2 Thin-Film As an Efficient Electrocatalyst for Hydrogen Evolution Reaction. *Chem. Commun.* **2015**, *51*, 7470−7473.

(12) Ma, Q.; Odenthal, P. M.; Mann, J.; Le, D.; Wang, C. S.; Zhu, Y.; Chen, T.; Sun, D.; Yamaguchi, K.; Tran, T.; et al. Controlled Argon Beam-Induced Desulfurization of Monolayer Molybdenum Disulfide. *J. Phys.: Condens. Matter* **2013**, *25*, 252201.

(13) Liu, T.; Premasiri, K.; Sui, Y.; Zhan, X.; Mustafa, H. A. B.; Akkus, O.; Zorman, C. A.; Gao, X. P. A.; Sankaran, R. M. Direct, Transfer-Free Growth of Large-Area Hexagonal Boron Nitride Films by Plasma-Enhanced Chemical Film Conversion (PECFC) of Printable, Solution-Processed Ammonia Borane. *ACS Appl. Mater. Interfaces* **2018**, *10*, 43936−43945.

(14) Yang, H.; Giri, A.; Moon, S.; Shin, S.; Myoung, J.-M.; Jeong, U. Highly Scalable Synthesis of MoS_2 Thin Films with Precise Thickness Control via Polymer-Assisted Deposition. *Chem. Mater.* **2017**, *29*, 5772−5776.

(15) Liu, K. K.; Zhang, W.; Lee, Y. H.; Lin, Y. C.; Chang, M. T.; Su, C. Y.; Lai, C. S.; et al. Growth of Large-Area and Highly Crystalline MoS_2 Thin Layers on Insulating Substrates. *Nano Lett.* **2012**, *12*, 1538−1544.

(16) Li, D. W.; Zou, Q. M.; Huang, X.; Rabiee Golgir, H.; Keramatnejad, K.; Song, J. F.; Xiao, Z. Y.; Fan, L. S.; Hong, X.; Jiang, L.; Silvain, J. F.; Sun, S.; Lu, Y. F. Controlled Defect Creation and Removal in Graphene and MoS_2 Monolayers. *Nanoscale* **2017**, *9*, 8997−9008.

(17) Joensen, P.; Crozier, E. D.; Alberding, N.; Frindt, R. F. A Study of Single-Layer and Restacked MoS_2 by X-ray Diffraction and X-ray Absorption Spectroscopy. *J. Phys. C: Solid State Phys.* **1987**, *20*, 4043−4053.

(18) Splendiani, A.; Sun, L.; Zhang, Y.; Li, T.; Kim, J.; Chim, C.-Y.; Galli, G.; Wang, F. Emerging Photoluminescence in Monolayer MoS_2. *Nano Lett.* **2010**, *10*, 1271−1275.

(19) Lee, C.; Yan, H.; Brus, L. E.; Heinz, T. F.; Hone, J.; Ryu, S. Anomalous Lattice Vibrations of Single- and Few-Layer MoS_2. *ACS Nano* **2010**, *4*, 2695−2700.

(20) Luo, S.; Hao, G.; Fan, Y.; Kou, L.; He, C.; Qi, X.; Tang, C.; Li, J.; Huang, K.; Zhong, J. Formation of Ripples in Atomically Thin MoS_2 and Local Strain Engineering of Electrostatic Properties. *Nanotechnology* **2015**, *26*, 105705.

(21) Chen, X.; Park, Y. J.; Kang, M.; Kang, S.-K.; Koo, J.; Shinde, S. M.; Shin, J.; Jeon, S.; Park, G.; Yan, Y.; MacEwan, M. R.; Ray, W. Z.; Lee, K.-M.; Rogers, J. A; Ahn, J.-H. CVD-Grown Monolayer MoS_2 in Bioabsorbable Electronics and Biosensors. *Nat. Commun.* **2018**, *9*, 1690.

(22) Behura, S.; Nguyen, P.; Che, S.; Debbarma, R.; Berry, V. Large-Area, Transfer-free, Oxide-Assisted Synthesis of Hexagonal Boron Nitride Films and Their Heterostructures with MoS_2 and WS_2. *J. Am. Chem. Soc.* **2015**, *137*, 13060−13065.

(23) Zhang, W.; Huang, J. K.; Chen, C. H.; Chang, Y. H.; Cheng, Y. J.; Li, L. J. High-Gain Phototransistors Based on a CVD MoS_2 Monolayer. *Adv. Mater.* **2013**, *25*, 3456−3461.

(24) Jeon, J.; Jang, S. K.; Jeon, S. M.; Yoo, G.; Jang, Y. H.; Park, J.-H.; Lee, S. Layer-controlled CVD Growth of Large-Area Two-Dimensional MoS_2 Films. *Nanoscale* **2015**, *7*, 1688−1695.

(25) Lim, Y. R.; Song, W.; Han, J. K.; Lee, Y. B.; Kim, S. J.; Myung, S.; Lee, S. S.; An, K. S.; Choi, C. J.; Lim, J. Wafer-Scale, Homogeneous MoS_2 Layers on Plastic Substrates for Flexible Visible Light Photodetectors. *Adv. Mater.* **2016**, *28*, 5025−5030.

(26) Lee, S.-K.; Lee, J.-B.; Singh, J.; Rana, K.; Ahn, J.-H. Drying-Mediated Self-Assembled Growth of Transition Metal Dichalcogenide Wires and Their Heterostructures. *Adv. Mater.* **2015**, *27*, 4142−4149.

(27) Conley, H. J.; Wang, B.; Ziegler, J. I.; Haglund, R. F., Jr.; Pantelides, S. T.; Bolotin, K. I. Bandgap Engineering of Strained Monolayer and Bilayer MoS_2. *Nano Lett.* **2013**, *13*, 3626−3630.

(28) Manzeli, S.; Allain, A.; Ghadimi, A.; Kis, A. Piezoresistivity and Strain-Induced Band Gap Tuning in Atomically Thin MoS_2. *Nano Lett.* **2015**, *15*, 5330−5335.

(29) Wang, Y.; Cong, C.; Qiu, C.; Yu, T. Raman Spectroscopy Study of Lattice Vibration and Crystallographic Orientation of Monolayer MoS_2 Under Uniaxial Strain. *Small* **2013**, *9*, 2857−2861.

(30) Liu, H.; Chi, D. Dispersive Growth and Laser-induced Rippling of Large-Area Single Layer MoS_2 Nanosheets by CVD on C-plane Sapphire Substrate. *Sci. Rep.* **2015**, *5*, 11756.

(31) Chen, R.; Yang, C.; Cai, W.; Wang, H.-Y.; Miao, J.; Zhang, L.; Chen, S.; Liu, B. Use of Platinum as the Counter Electrode to Study the Activity of the Nonprecious Metal Catalysts for the Hydrogen Evolution Reaction. *ACS Energy Lett.* **2017**, *2*, 1070−1075.

(32) Shinagawa, T.; Garcia-Esparza, A. T.; Takanabe, K. Insight on Tafel Slopes from A Microkinetic Analysis of Aqueous Electrocatalysis for Energy Conversion. *Sci. Rep.* **2015**, *5*, 13801.

(33) Benck, J. D.; Hellstern, T. R.; Kibsgaard, J.; Chakthranont, P.; Jaramillo, T. F. Catalyzing the Hydrogen Evolution Reaction (HER) with Molybdenum Sulfide Nanomaterials. *ACS Catal.* **2014**, *4*, 3957−3971.

(34) Soon, J. M.; Loh, K. P. Electrochemical Double-Layer Capacitance of MoS_2 Nanowall Films. *Electrochem. Solid-State Lett.* **2007**, *10*, A250−A254.